

Real-Time Imaging of Quantum Entanglement

Robert Fickler^{1,2,*}, Mario Krenn^{1,2}, Radek Lapkiewicz^{1,2}, Sven Ramelow^{1,2},
Anton Zeilinger^{1,2,3,*}

¹Quantum Optics, Quantum Nanophysics, Quantum Information, University of Vienna,
Boltzmanngasse 5, Vienna A-1090, Austria

²Institute for Quantum Optics and Quantum Information, Austrian Academy of Science,
Boltzmanngasse 3, Vienna A-1090, Austria

³Vienna Center for Quantum Science and Technology, Faculty of Physics, University of Vienna,
Boltzmanngasse 5, Vienna A-1090, Austria

*Correspondence to: robert.fickler@univie.ac.at and anton.zeilinger@univie.ac.at

Quantum Entanglement – correlations between at least two systems that are stronger than classically explainable^{1,2} – is widely regarded as one of the most prominent features of quantum mechanics and quantum information science³. Although, the creation of entanglement between two systems has become possible in laboratories, it has been out of the grasp of one of the most natural ways to investigate nature: direct visual observation. Here we show that modern imaging technology, namely a triggered intensified charge coupled device (ICCD) camera, is fast and sensitive enough to image in real-time the influence of the measurement of one photon on its entangled partner. To demonstrate the non-classicality of the measurements quantitatively from the registered intensity we develop a novel method to statistically analyze the image and precisely quantify the number of photons within a certain region. In addition, we show the high flexibility of our experimental setup in creating any desired spatial-mode entanglement, even with arbitrary combinations of two mode families. Our results suggest that visual imaging in quantum optics and quantum information science provides a new intuitive understanding of entanglement and will improve various technological applications of quantum science.

A fairly young but vibrant field that studies the spatial structure of the optical modes of photons (e.g. Laguerre-Gauss⁴, Ince-Gauss⁵, Bessel-Gauss⁶) continues to attract wide interest. Each spatial mode offers many interesting features, like orbital angular momentum⁷ or continuous vortex splitting⁸, which already lead to novel insights in quantum optics like higher dimensional entanglement^{9,10,11,12}, novel uncertainty relations for the angular and OAM degree-of-freedom^{13,14} or angular sensitivity enhancement with very high OAM¹⁵. In our experiment, we use a combination of the polarization and spatial degree-of-freedom (DOF) to be able to directly image entanglement. We start with a high-fidelity polarization-entangled two-photon state (Figure 1). One photon is unchanged; the other photon is brought to a second setup, which transfers the polarization DOF to a specific chosen spatial mode¹⁵. In this interferometric setup, the photons get transferred by a liquid-crystal spatial light modulator, dependent on their polarization (methods), to a hybrid-entangled two-photon state

$$|\psi\rangle = \alpha|H\rangle|spM_1\rangle + e^{i\phi}\beta|V\rangle|spM_2\rangle, \quad (1)$$

where α , β , and Φ are real and $\alpha^2 + \beta^2 = 1$, H and V denote the horizontal and vertical polarization, spM_1 and spM_2 correspond to arbitrary spatial modes, and the positions of the ket-vectors label the different photons. In order to image the created spatial mode and demonstrate entanglement between the two photons, the polarization encoded photon is projected onto a certain polarization and detected by a single photon detector. The signal from the detector is used as a trigger for the ICCD camera, which in turn registers the transferred photon.

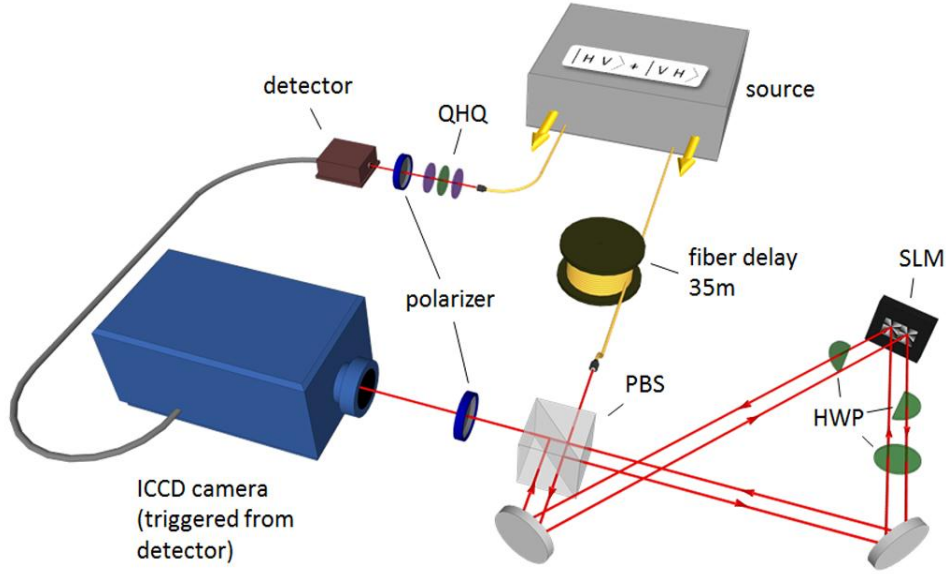


Figure 1: Sketch of the experimental setup. Polarization entanglement is created in a SPDC process (source – grey box) and both photons are coupled into single mode fibers (yellow). One photon is measured in the polarization bases with a combination of two quarter wave plates, a half wave plate (QHQP – violet and green) and a polarizer (blue). The photon is detected by single photon detector (brown) and the detector signal is used as a trigger for the ICCD camera. The second photon is delayed by a 35m fiber and brought into the interferometric transfer setup, which consists of a polarizing beam splitter (PBS), three half wave plates (HWP – green), a spatial light modulator (SLM - black) and a polarizer (blue) at 45° after the interferometer. In the transfer setup the HWPs rotate polarization to ensure the optimal working of the SLM and to separate the output from the input path. Depending on the polarization the photon gets transferred by the SLM to any desired spatial mode. The polarizer after the interferometer erases any information to which spatial mode the photon was modulated and thus completes the transformation. The spatial mode of the photon is registered by the triggered ICCD camera which is gated for 5ns and therefore only detects the transferred photons which belong to polarization encoded trigger photons.

The rapid progress in imaging technologies over the last few years has made CCD cameras an interesting option for single photon detection in quantum optics experiments, since the spatial information is directly accessible. Due to quantum efficiencies of up to 90%, electron multiplied CCD cameras have attracted attention recently and have been used to show non-classical

correlations directly from photons produced via spontaneous parametric down conversion (SPDC)^{16,17,18,19}. The downside of such cameras is that they only allow relatively long exposure times (μs) which makes it necessary to sum over many images with a sparse number of photons to detect signatures of entanglement. Furthermore, this μs exposure time makes it unfeasible to use them for coincidence imaging of entanglement where precise and fast timing is essential. In contrast, ICCD cameras have lower quantum efficiencies due to the intensifier and fluorescence screen in front of the CCD chip but show a very good signal to noise ratio and therefore good single photon sensitivity. They have been used in many experiments to show non-classical effects of the photons from the SPDC process^{20,21,22,23,24}. The biggest advantage of ICCD cameras is the very fast ($\sim 2\text{ns}$) and precise ($\sim 10\text{ps}$) optical gating of the intensifier which makes it possible to use them in a coincidence scheme for real time imaging of quantum entanglement. In our measurements, we use an ICCD (Andor iStar A-DH334T-18F-03) with a quantum efficiency of 3% for 810nm wavelength and a gating of 5ns to observe clear single-photon images even for very complex mode structures (Figure 2 b and Figure 4). Note that ICCD cameras with 20% efficiency and 2ns gating, which are readily available, promise a 20-fold increase in the signal to noise ratio. On the camera the one photon event is distributed over more pixels of the CCD because each channel of the intensifier is bigger than the CCD pixels and therefore spread over many pixels. Since the adjustable insertion delay time for triggering the ICCD is at least 35ns, we delay the second photon with a 35m long fibre before sending it through the transfer setup. If a wrong delay is chosen no image of the light mode can be seen at the camera. This demonstrates that only those photons which belong to a polarization encoded partner photon, are visible and nearly no accidental photon events contribute to the image (see Figure 2 a bottom right). Thus no post-selection or correction has to be applied. A few residual events appear due to the high triggering rate (MHz) and the resulting thermal noise from the intensifier or from the afterglowing of the fluorescing phosphorous screen. We find the ratio of these residual events (wrong delay) to the number of photon events in a picture to be on the order of 1:75. Those undesirable residual events may be suppressed substantially, with more efficient ICCD cameras and/or a smaller gating times.

To visualize the effect of entanglement, we scan the Poincaré sphere of the polarization encoded trigger photon and register the appearing mode pattern from the transferred photons at the ICCD camera. In this way, the whole Bloch sphere for the spatial mode of the transferred photon can be imaged (Figure 2 a). Since the measurement of each spatial mode only takes a few seconds (e.g. 3 seconds for $\text{LG}_{\pm 1}$), the influence of the polarization measurement of the first photon is visible in real time at the ICCD camera (Supplementary movie 1). Entanglement is already visible in this video, since the high-contrast minima and maxima shift in very good correspondence to the polarization angle measured on the partner photon. In Figure 2 b images of the detected higher order LG modes up to $\text{LG}_{\pm 100}$ can be seen.

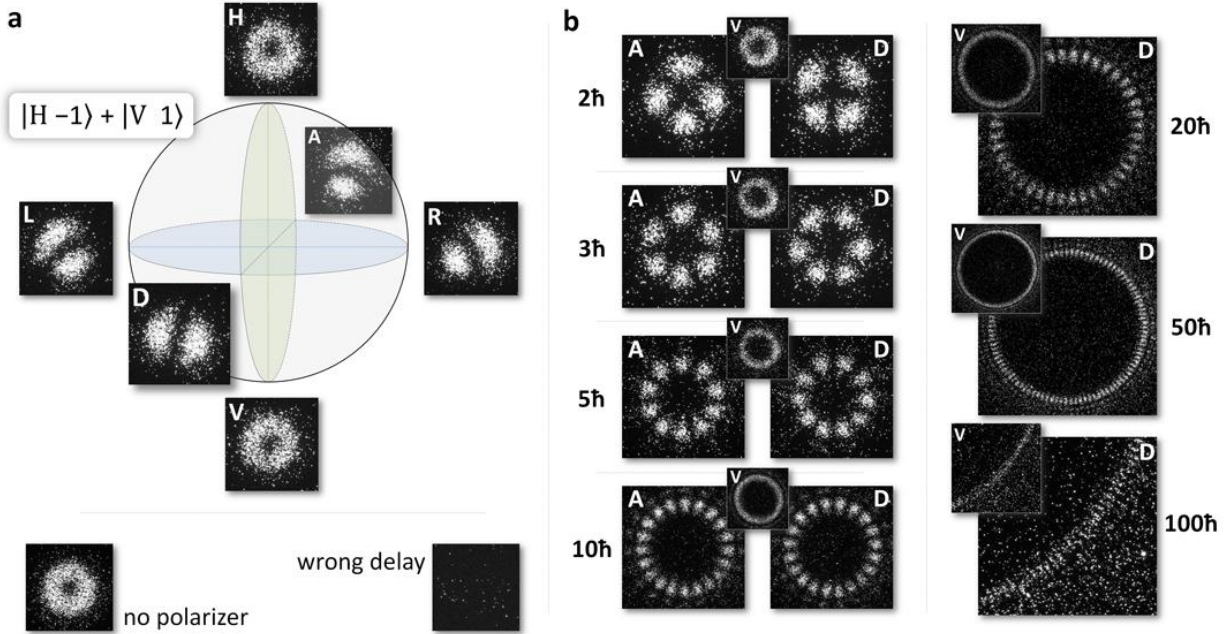


Figure 2: Gallery of single photon images where the photons are transferred to different orders of LG modes. Depending on which polarization the entangled trigger photon is projected (white letters in the images), different mode patterns are registered with ICCD camera. (a) shows a Bloch sphere for the first order Laguerre-Gauss modes. By scanning the polarization encoded trigger photon around its Poincaré sphere, the whole LG-Bloch sphere of the entangled partner photon in the spatial mode can be visualized in real time. A sequence of single-photon images for different trigger polarizations around a meridian (green circle in the sphere) and the equator (blue circle in the sphere) confirms directly the presence of entanglement due to the high-contrast minima and maxima for the two mutually unbiased bases and can be seen in the Supplementary movie 1. If no polarizer is put in the path of the trigger photon (bottom left) a statistical mixture of all states of the LG-Bloch sphere is registered. If the delay is changed to a wrong value by 10ns (bottom right) and therefore the gating time of the ICCD camera does not match to the arrival of the delayed photons, nearly no intensity is registered. (b) Although the structure of the superposition for higher order LG modes becomes more complicated and the resolution of the SLM and the camera is getting crucial, the characteristic petal structure can be identified even up to the 100th order where a single photon carries 100 quanta of OAM.

While visual observation already intuitively confirms the presence of entanglement, we demonstrate it quantitatively by simulating the number of photons dependent on the registered intensity per angular region and precisely evaluating its error margin (methods). For this purpose, we reconstruct from 5790 single photon events the probability distribution of registered counts at the ICCD per detected photon (Figure 3 a). With this camera-specific probability function, it is possible to Monte Carlo simulate the number of photons and the error margin for any measured intensity image from the ICCD (Figure 3 b).

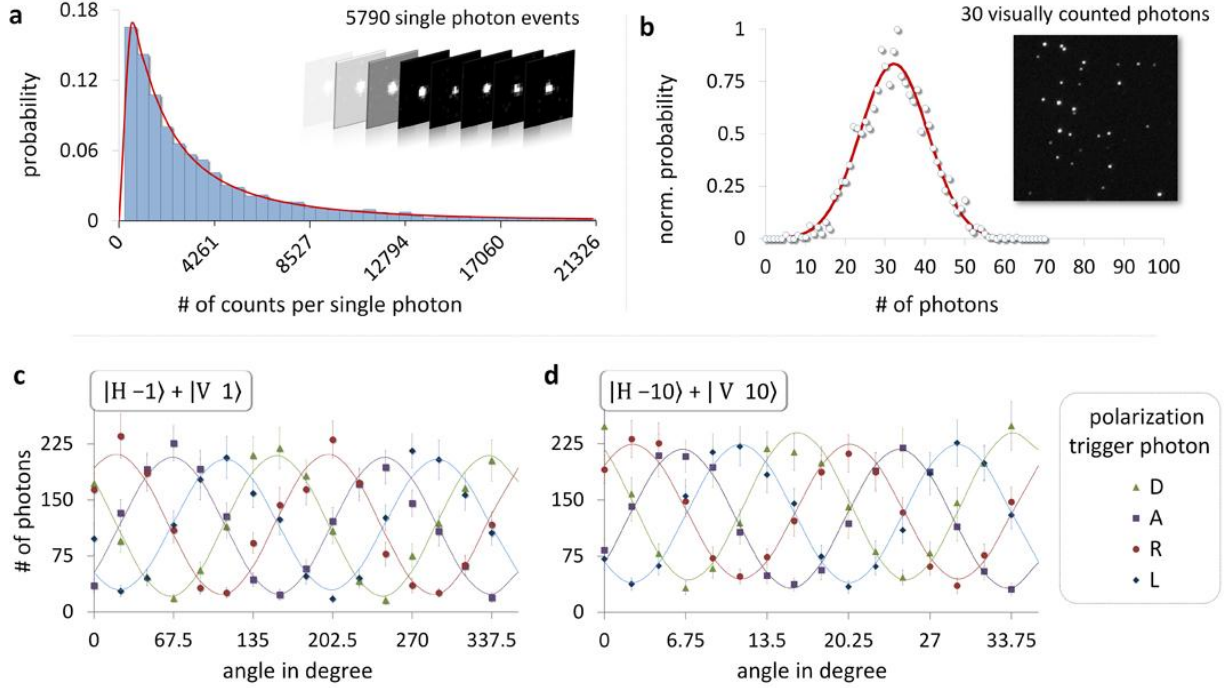


Figure 3: Simulation of the photon number from a registered intensity image. (a) shows the measured histogram of registered counts at the ICCD for 5790 single photon events. A log-normal distribution was fitted to the data which is specific to the ICCD camera we used. (b) For the example image (inset) the simulation of the photon number was performed and the normalized probability is shown in the graph. A Gaussian fit leads to a simulated value of 32 photons with a 1σ -error of ± 9 photons, while 30 photons can be counted visually. (c and d) To demonstrate entanglement quantitatively with the introduced method, we simulate the number of photons per angular region from registered intensity images of the ICCD camera for different polarizations of the trigger photon. From the simulated number of photons in the minima and maxima of the fringes, the visibilities are calculated and used to violate the separability bound of an entanglement witness. Because of the periodic structure of LG superpositions all angular regions in multiples of $\frac{360^\circ}{2l}$ are summed up to get a bigger number of photons per angle and therefore a better statistical significance, especially for higher order modes.

To confirm entanglement we make use of a specific feature of the Laguerre-Gauss (LG) mode family. The spatial structure of two superimposed LG modes with opposite helicities $|LG_{\pm l}\rangle = |LG_l\rangle + e^{i\varphi}|LG_{-l}\rangle$ shows a radially symmetric distribution where a change of the phase φ between the two modes directly translates to a spatial rotation of $\frac{\varphi}{2l} \frac{360^\circ}{2\pi}$. To discriminate between different orientations of the structure and therefore different superpositions¹⁵, we simulate the photon number per angular region from the measured intensity image for different trigger polarizations (Figure 3 c and d). From the maximal and minimal detected photon numbers the visibilities in two mutually unbiased bases and therefore the expectation value of an entanglement witness operator \hat{W} can be calculated²⁵ (supplementary information). For all separable states the inequality

$$\hat{W} = vis_{D/A} + vis_{R/L} \leq 1 \quad (2)$$

holds. Capital letters stand for the polarization of the trigger photon (D = diagonal, A = anti-diagonal, R = right circular, L = left circular). Measured correlations which add up to a value bigger than 1 demonstrate entanglement. For first order LG modes with $l=\pm 1$ we obtained a value of 1.64 ± 0.04 which violates the inequality (2) by more than 15 standard deviations, therefore proving entanglement. For $LG_{\pm 2}$, $LG_{\pm 3}$, $LG_{\pm 5}$ and $LG_{\pm 10}$ the measured witnesses are 1.48 ± 0.08 , 1.46 ± 0.08 , 1.47 ± 0.07 , and 1.42 ± 0.07 respectively and thus violate the bound for separable states by more than 5 standard deviations. We note that the simulated photon numbers might be a bit smaller than they were in the actual measurement, due to saturation effects of the camera where a lot of photons are registered in the same region namely the maxima. However, a bigger actual photon number in the maximum would correspond to a higher value of the visibility and therefore a stronger violation than the one presented here.

Recently, it was shown that hybrid-entangled two-photon states of higher-order LG modes can be used to improve sensitivity in the remote sensing of an angular rotation¹⁵. This gear-like behaviour between the rotation of the polarization and the petal structure of the spatial mode can be visualized with the ICCD camera. A scan of the polarization around the equator of the trigger photons' Poincare sphere leads to a rotation of the structure by 180° for $LG_{\pm 1}$, 90° for $LG_{\pm 2}$ and 36° for $LG_{\pm 5}$ (Supplementary movie 2).

To demonstrate the flexibility of the setup, we transfer one of the photons to the Hermite-Gauss (HG) mode family and the general family of Ince-Gauss (IG) modes (Figure 4 a and b). All registered single-photon images show a very good agreement with the theoretical prediction. Furthermore, the transfer setup is able to create entanglement between polarization and an artificial mixture of two different mode families at the same time (see Figure 4 c). By transferring the photon to a superposition of a higher order LG and HG mode it only carries quanta of OAM if the trigger photon is projected in the vertical polarization. If the trigger photon is found in the horizontal polarization the entangled partner photon will be in the HG mode without OAM, which could be used to remotely determine the OAM content of distant photon dependent onto which polarization the unchanged photon is projected.

Our result demonstrate the first visualization of entanglement in real-time. This offers the possibility to directly observe the influence of one system on the entangled, distant partner system which apart from enabling a better use of the spatial DOF in quantum optics experiments may help for a more intuitive understanding of entanglement. The presented method of simulating the amount of photons corresponding to a given intensity registered by the camera opens up novel experimental possibilities to determine more efficiently the structure and properties of spatial modes from only one single intensity image. Additionally, we demonstrated the flexibility of the transfer setup in its capability to create custom tailored spatial mode entanglement where one photon can even be in a superposition of different mode families.

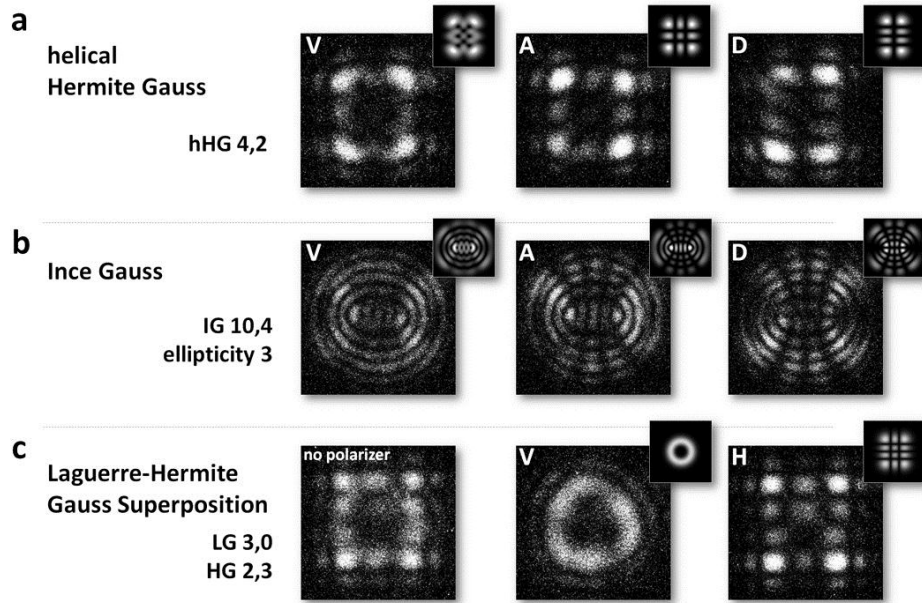


Figure 4: Gallery of registered single photon images where the transferred photon is encoded in different HG, IG, and LG/HG modes which demonstrates the flexibility of the transfer setup in creating any desired spatial mode entanglement. The white letters in each image depict to which polarization the entangled trigger photon was projected and the small insets above each image correspond to the theoretical expected intensity structure of the transferred photon. (a) For the helical HG mode family²⁶ a trigger photon in diagonal (D) or anti-diagonal (A) polarization leads to different orders of HG modes for the images of the entangled partner photon. (b) If the photon is transferred to the general family of IG modes characteristic properties like splitting of the vortices (vertical (V) polarized trigger photons) or additional nodal lines (D or A polarized trigger photons) can be seen. (c) The artificial superposition between the mode families of LG with OAM and HG without OAM shows that any custom tailored spatial mode entanglement can be realized.

Methods

Source and spatial light modulator (SLM):

The polarization-entangled photon pairs were created in a SPDC process using a 15mm-long type-II nonlinear crystal (periodically poled potassium titanyl phosphate (ppKTP)) in a Sagnac-type configuration^{27,28}. A blue 405nm continuous-wave diode laser with up to 35mW of power pumps the crystal and thereby creates photon pairs of 810nm wavelength. Two 3nm band-pass filters were used before the photons were coupled into single-mode fibers. With this approximately 1.3 million pairs per second can be detected at full pump power. Any polarization change between the source and the transfer setups are undone by fiber polarization controllers. The SLM (resolution: 1920x1080, pixel size: 8 μ m, Holoeye Photonics AG) in the transfer setup, which modulates only the phase of the light, was used to create the desired spatial modes.

Simulating the number of photons

For the simulation of the photon number from the registered intensity at the ICCD camera, we need to know the probability distribution of those counts caused by single photon events. To achieve this we measured the registered counts at the ICCD of 5790 single photons. In each shot we subtracted the mean background (readout noise) of each pixel and counted all the detected counts of a contiguous pixel array as one photon where at least one pixel value is above 5 standard deviations from the background fluctuations. From those measurements a histogram can be obtained, which is specific to the ICCD camera we used. A very good fit to the resulting histogram was obtained by using a log-normal probability function. In order to reconstruct the actual photon number from the amount of registered counts, we use this probability function to perform a Monte Carlo simulation. For each possible photon number 50000 different combinations of counts are simulated and compared to the value detected experimentally with the camera. By counting the times when the simulated value lies within a certain interval (here the width of the histogram bins) the probabilities of each photon number can be found. From a Gaussian fit to the resulting distribution we obtain the photon number and its error for each detected number of counts.

References

1. Einstein, A., Podolsky, B. & Rosen, N. Can quantum-mechanical description of physical reality be considered complete?, *Phys. Rev.* **47**, 777–780 (1935).
2. Bell, J. S., On the Einstein Podolsky Rosen paradox, *Physics* **1**, 195-200 (1965).
3. Horodecki, R., Horodecki, P., Horodecki, M. & Horodecki, K. Quantum entanglement, *Rev. Mod. Phys.* **81**, 865-942 (2009).
4. Mair, A., Vaziri, A., Weihs, G. & Zeilinger, A. Entanglement of the orbital angular momentum states of photons. *Nature* **412**, 313-316 (2001).
5. Krenn, M., Fickler, R., Huber, M., Lapkiewicz, R., Plick, W., Ramelow, S. & Zeilinger, A. Entanglement of photons with tunable singularities, *arXiv:1205.2514* (2012) <<http://arxiv.org/abs/1205.2514>>
6. McLaren, M., Agnew, M., Leach, J., Roux, F.S., Padgett M. J. & Forbes A. Entangled Bessel-Gaussian beams, *Optics Express*, **20**, 21, 23589-23597 (2012).
7. Allen, L., Beijersbergen, M. W., Spreeuw, R. J. C. & Woerdman, J. P. Orbital angular momentum of light and the transformation of Laguerre-Gaussian laser modes. *Phys. Rev. A* **45**, 8185–8189 (1992).
8. Bandres, M. A. & Gutiérrez-Vega, J. Ince Gaussian beams. *Optics Letters* **29**, 144–146 (2004).

9. Vaziri, A., Weihs, G. & Zeilinger, A. Experimental two-photon, three-dimensional entanglement for quantum communication. *Phys. Rev. Lett.* **89**, 240401 (2002).
10. Langford, N. K., Dalton, R. B., Harvey, M. D., O'Brien, J. L., Pryde, G. J., Gilchrist, A., Bartlett, S. D. & White, A. G. Measuring entangled qutrits and their use for quantum bit commitment, *Phys. Rev. Lett.* **93**, 053601 (2004).
11. Dada, A. C., Leach, J., Buller, G. S., Padgett, M. J. & Andersson, E. Experimental high-dimensional two-photon entanglement and violations of generalized Bell inequalities. *Nature Physics* **7**, 677–680 (2011).
12. Salakhutdinov, V.D., Eliel, E.R. & Löffler, W. Full-field quantum correlations of spatially entangled photons, *Phys. Rev. Lett.* **108**, 173604 (2012).
13. Jack, B. *et al.* Demonstration of the angular uncertainty principle for single photons. *Journal of Optics* **13**, 064017 (2011).
14. Leach, J. *et al.* Quantum correlations in optical angle–orbital angular momentum variables, *Science* **329**, 662–665 (2010).
15. Fickler, R., Lapkiewicz, R., Plick W. N., Krenn, M., Schöff C., Ramelow S. & Zeilinger A. Quantum entanglement of high angular momenta, *Science* **338**, 640–643 (2012).
16. Blanchet, J.-L., Devaux, F., Furfaro, L. & Lantz, E. Measurement of sub-shot-noise correlations of spatial fluctuations in the photon-counting regime. *Phys. Rev. Lett.* **101**, 233604 (2008).
17. Brida, G., Genovese, M. & Ruo Berchera, I. Experimental realization of sub-shot-noise quantum imaging. *Nature Photonics* **4**, 227–230 (2010).
18. Moreau, P.-A., Mougin-Sisini, J., Devaux, F. & Lantz, E. Realization of the purely spatial Einstein-Podolsky-Rosen paradox in full-field images of spontaneous parametric down-conversion, *Phys. Rev. A* **86**, 010101 (2012).
19. Edgar, M.P. *et al.* Imaging high-dimensional spatial entanglement with a camera, *Nature Communications* **3**, 984 (2012).
20. Jost, B. M., Sergienko, A. V., Abouraddy, A. F., Saleh, B. E. A. & Teich, M. C. Spatial correlations of spontaneously down-converted photon pairs detected with a single-photon-sensitive CCD camera, *Optics Express* **3**, 2, 81–88 (1998).
21. Abouraddy, A. F., Nasr, M. B., Saleh, B. E. A., Sergienko, A. V. & Teich, M. C. Demonstration of the complementarity of one- and two-photon interference. *Phys. Rev. A* **63**, 063803 (2001).
22. Jedrkiewicz, O. *et al.* Detection of sub-shot-noise spatial correlation in high-gain parametric down conversion. *Phys. Rev. Lett.* **93**, 243601 (2004).

23. Di Lorenzo Pires, H., Monken, C. H. & van Exter, M. P. Direct measurement of transverse-mode entanglement in two-photon states. *Phys. Rev. A* **80**, 022307 (2009).
24. Aspden, R. S., Tasca, D. S., Boyd, R. W. & Padgett, M. J. Heralded single-photon ghost imaging. *Submitted*
25. Gühne, O. & Tóth, G. Entanglement detection. *Physics Reports* **474**, 1–75 (2009).
26. López-Mariscal, C. & Gutiérrez-Vega, J. C. Propagation of helical Hermite-Gaussian beams. *SPIE Annual Meeting, SPIE Vol. 6663: Laser Beam Shaping VIII*, 666307 (2007).
27. Kim, T., Fiorentino, M. & Wong, F. N. C. Phase-stable source of polarization-entangled photons using a polarization Sagnac interferometer *Phys. Rev. A* **73**, 012316 (2006).
28. Fedrizzi, A., Herbst, T., Poppe, A., Jennewein, T. & Zeilinger A. A wavelength-tunable fiber-coupled source of narrowband entangled photons, *Optics Express* **15**, 23, 15377-15386 (2007).

Supplementary Material

Movie 1 and movie 2 files attached

Calculation of the entanglement witness

The introduced entanglement witness consists of the sum of two visibilities vis

$$\hat{W} = vis_{D/A} + vis_{R/L} , \quad (3)$$

where the indices describe the polarization of the trigger photon. It can be calculated as follows: Because the phase between the LG mode with a positive OAM quantum number l and negative OAM value $-l$ is directly connected to the angular position via the formula $\gamma = \frac{\varphi}{2l} \frac{360^\circ}{2\pi}$, it is possible to distinguish between any equally weighted superposition of Laguerre-Gauss states

$$|LG_{\pm l}\rangle = \frac{1}{\sqrt{2}} |LG_l\rangle + e^{i\varphi} |LG_{-l}\rangle \quad (4)$$

with the ICCD camera. The two visibilities of the witness operator can be rewritten in terms of four projections onto different trigger polarizations and angular positions. Hence, the witness becomes

$$\hat{W} = (\hat{P}_{D,\gamma_1} + \hat{P}_{A,\gamma_1^\perp} - \hat{P}_{D,\gamma_1^\perp} - \hat{P}_{A,\gamma_1}) + (\hat{P}_{R,\gamma_2} + \hat{P}_{L,\gamma_2^\perp} - \hat{P}_{R,\gamma_2^\perp} - \hat{P}_{L,\gamma_2}) , \quad (5)$$

where the position of the indices label the two photons, the capital letters stand for the trigger polarization and the γ stands for the angular position of the registered structure at ICCD. γ_1 can be chosen to fit to the maximum intensity for D polarized trigger photons and thus fixes all following angular positions of the LG superposition measurements. The angle $\gamma_2 = \gamma_1 + \frac{45^\circ}{l}$ therefore corresponds to the second mutually unbiased basis which is needed to verify entanglement. The \perp -sign illustrates the angular position of the respective orthogonal superposition e.g. $\gamma_1^\perp = \gamma_1 + \frac{90^\circ}{l}$ which is necessary to measure the visibility. To find the bound for all separable states we use the general pure separable two photon OAM state where the first photon is in the polarization mode and the second photon in the LG mode

$$|\psi\rangle = (a|H\rangle + b \cdot e^{i\varphi_1}|V\rangle) \otimes (c|LG_l\rangle + d \cdot e^{i\varphi_2}|LG_{-l}\rangle) , \quad (6)$$

with $a, b, c, d, \varphi_1, \varphi_2 \in \mathbb{R}$, $a^2 + b^2 = 1$, $c^2 + d^2 = 1$ and l denotes the quanta of OAM. The straightforward calculation of the witness (5) for the separable state (6) leads to

$$\hat{W} = 4 \cdot a \cdot b \cdot c \cdot d \cdot \cos(\varphi_1 - \varphi_2) . \quad (7)$$

Therefore, the maximal value of the witness \hat{W} is 1 for $a=b=c=d=\frac{1}{\sqrt{2}}$ and $\varphi_1 = \varphi_2$. If the sum of the visibilities is bigger than 1 the measured state is non-separable or in other words entangled:

$$\hat{W} = vis_{D/A} + vis_{R/L} \begin{cases} \leq 1 & \text{separable} \\ > 1 & \text{entangled} \end{cases}$$

Note that the presented witness is linear and therefore the calculated bound holds for all separable mixed states as well.